Nanoscale Advances

ROYAL SOCIETY OF CHEMISTRY

PAPER

View Article Online
View Journal | View Issue



Cite this: *Nanoscale Adv.*, 2025, **7**, 2329

# Without a grain of salt: micropatterning clean MXene thin-film electronics†

Bar Favelukis,[a] Barak Ratzker,[a] Rebeca Miyar,[a] Jürgen Jopp,[b] Alexander Upcher,[b] Pini Shekhter,[c] Nitzan Maman[b] and Maxim Sokol *[a]

MXenes exhibit remarkable electrical, mechanical, and thermal properties, positioning them as strong candidates for high-performance electrodes and interconnects. Deposited 2D MXene thin-films suffer from a persistent issue of crystalline salt residues that originate from dissolved intercalation salts used for the exfoliation process during synthesis. These 3D salt by-products can cause issues during further nanofabrication processing and be detrimental to integrated device performance. This study introduces a three-step approach involving spin-coating deposition, HCl spin-cleaning, and lift-off. Rigorous morphological characterization of the patterned MXene was performed, confirming that the spin-cleaning step effectively removed all halide salt residues. Transparent sub-10 nm-thick MXene thin-film electrodes, down to a width of 5 μm with ~1.5 μm resolution, were produced. The electrical properties were probed, showcasing exceptional conductivity (~1350 S $cm^{-1}$ for a 50 μm-wide electrode) with high photosensitivity at the MXene–Si junction. The proposed method yields clean patterned MXene thin films, enabling easier integration of MXene or other 2D materials into future microelectronic devices.

Received 26th November 2024
Accepted 4th February 2025

DOI: 10.1039/d4na00983e

rsc.li/nanoscale-advances



## 1. Introduction

Technological advancements and device miniaturization in microelectronics continuously push the limits of current materials capabilities.[1] As integrated circuits become more powerful or feature smaller components, conventional metal interconnects face significant challenges, including high resistivity, electromigration, and reliability issues.[2] The need to replace traditional metal electrodes and interconnects is driven further by the demand for transparent, flexible, and wearable electronics. A promising solution is the thin-film deposition of 2D inorganic materials for next-generation electronics.[3] Currently, most low-dimensional electrode materials face significant challenges related to high synthesis temperatures and limitations in scalable manufacturing.[4–7]

MXenes, an emerging diverse family of 2D transition metal carbides/nitrides, are a promising alternative to overcome said challenges.[8–10] The synthesis of MXene involves selectively etching the "A" element out of the MAX phases to form the general formula $M_{n+1}X_nT_z$ ($n$ = 1–4), where "M" is an early transition metal, "X" represents carbon or nitrogen, and "$T_z$" represents surface terminations, usually –O, –OH, or –F.[11] Colloidal solutions of single-layer MXene are prepared by exfoliation of multilayer MXene intercalated with halide or organic salts (*e.g.*, LiF, LiCl, TMAOH, *etc.*) during or after etching.[11]

Unlike other 2D materials, MXene can be synthesized in large batches and directly exfoliated into a colloidal solution, simplifying processing scalability and avoiding complex surface modification requirements.[12,13] MXenes are known for their high electrical conductivity and have been shown to withstand high breakdown current densities (~1.2 $10^8$ A $cm^{-2}$).[2] Another advantage is the tunability of their work function, for example $Ti_3C_2T_z$ can exhibit a work function ranging from 3.9 to 4.8 eV, depending on surface terminations.[14,15] Precisely controlling the thickness of the deposited MXene thin films (<20 nm) enables fabrication of transparent microelectronic components with high conductivity.[16,17] To realize MXene-based microelectronics a variety of deposition methods can be employed.[18] MXene deposition can be performed using spray coating,[19] dip coating,[20] blade coating,[21] inkjet printing,[22] and spin coating.[22,23] Followed by patterning techniques such as reactive ion etching,[24] deposition over a photoresist and subsequent lift-off,[25–27] and microscale contact printing.[28]

The deposition of MXene films requires using MXene colloids that contain unavoidable traces of dissolved halide salts (used for intercalation).[11] Therefore, once the MXene colloid dries up, salt residues always crystallize on the MXene

[a]*Department of Materials Science and Engineering, Tel Aviv University, P. O. B. 39040, Ramat Aviv 6997801, Israel. E-mail: sokolmax@tauex.tau.ac.il*

[b]*Ilse Katz Institute for Nanoscale Science and Technology, Ben-Gurion University of the Negev, P. O. B. 653, Beer-Sheva 8410501, Israel*

[c]*Tel Aviv University Center for Nanoscience and Nanotechnology, Tel Aviv University, P. O. B. 39040, Ramat Aviv 6997801, Israel*

† Electronic supplementary information (ESI) available. See DOI: https://doi.org/10.1039/d4na00983e

films.[16,18,26,29–31] This issue is currently overlooked as the salt residues sit on top of the film and have a negligible effect on the performance of the MXene itself. However, the presence of salt residues will present challenges for future integration of MXenes with other materials in more complex integrated 2D microelectronic systems. The salt crystals 3D structure obstructs 2D layered construction and their high volatility can be extremely detrimental during nanofabrication processes at elevated temperatures.[31] In addition, alkali metal (*e.g.*, Li) and other contaminations (*e.g.*, F) can alter desired electronic properties and even lead to catastrophic failure of the electronic device.[31] Therefore, integrating a step to eliminate salt residues during the fabrication process is imperative.

Previous studies have demonstrated deposition and patterning of MXene films,[24,25,27,28,32–34] however almost none have addressed the issue of salt residues.[35] In addition, lift-off related morphological defects, nor the electrical properties of microscale features have only been superficially addressed.[18] Herein we demonstrate an effective spin-coating fabrication process for MXenes that involves a subsequent salt removal step by spin cleaning using HCl. The microstructure of the obtained MXene micropatterned features were characterized in-depth and the microscale electronic properties were assessed.

# 2. Experimental section

## 2.1 Materials synthesis

**2.1.1 MAX phase.** $Ti_3AlC_2$ powder was synthesized through a high temperature liquid-phase reaction. Titanium carbide (TiC 99.5%, Alfa Aesar), titanium (Ti 99.7%, Strem), aluminum (Al 99.7%, Strem) powders were mixed in a ratio of 2 : 1 : 1.1 and tumbled in a 50 ml centrifuge tube with stainless steel balls at 200 rpm for 18 h. The mixed powders were then cold pressed in a 20 mm die at 1.5 tons, and the resulting pellet was placed in an alumina crucible. The pellet underwent heat treatment in a tube furnace at 1500 °C for 3 h, with a heating rate of 5 °C $min^{-1}$, under an Ar pressure of 200 sccm. Following the heat treatment, the pellet was ball-milled at 1800 rpm for 5 min and subsequently ground and sieved resulting in a ≥300 mesh powder.

**2.1.2 MXene.** $Ti_3C_2T_z$ MXene was synthesized by selectively etching the Al layer from the $Ti_3AlC_2$ MAX phase precursor. The acid solution was prepared by dissolving 1.6 g of lithium fluoride (LiF 99%, Strem) in 20 ml of hydrochloric acid 10.2 M (HCl 32%, Bio-Lab) in a high-density polyethylene vial with a magnetic stirrer. Then, 1 g of MAX powder was slowly added to the solution. The etching process was carried out while being held at 45 °C in an oil bath for 24 h. After the etching process, the mixture was centrifuged at 3500 rpm, twice in 0.5 M HCl followed by several times in DI water until the pH reached 6 (and the multilayer MXene became suspended). To exfoliate the MXene the suspension was then sonicated in an ultrasonic bath for 1 h while being kept at 15 °C by active cooling. After sonication the suspension was centrifuged at 3500 rpm for 30 min to separate any unexfoliated sediment. The MXene colloidal solution was bubbled with $N_2$ and stored at 4 °C. Finally, 5 ml of the colloid was dried and weighed to determine the MXene load which was roughly 11 g $l^{-1}$.

## 2.2 MXene deposition and patterning

Various substrates were prepared for MXene coating. A sapphire wafer (*c*-plane sapphire EPI ready, Semiconductor Wafer Inc., SWI), microscope glass slide (1–1.2 mm, Huida Medical Instruments Co.,Ltd), and Si wafer (100 n-type p-doped 1–100 Ω cm, University wafers) were diced into 8 × 8 mm square substrates using a dicer (Disco DAD 3350). In addition, n-type Si wafers with developed photoresist (AZ1518 MicroChemicals) were diced into 1 × 1 cm squares substrates. Following dicing all the substrates were sonicated in DI water for 7 min to remove any dicing residues. Before coating, the sapphire, glass, and Si were cleaned with piranha solution 1 : 3 $H_2O_2/H_2SO_4$, respectively, ($H_2SO_4$ 98% SDFCL, $H_2O_2$ 35% ThermoFisher Scientific) and the and Si wafers with developed photoresist were cleaned with diluted piranha solution (1 : 3 piranha/$H_2O$) for 15 min, then rinsed in DI water and dried with compressed $N_2$. MXene solutions with loading between 0.1 and 7 g $l^{-1}$ were prepared and spin-coated on the Si substrates at 2000 or 3000 rpm for 90 s using a spin-coater (Specialty Coating Systems, INC Spincoater Model P6700). The sapphire and glass substrates were spin-coated with MXene solutions of 7 g $l^{-1}$ at 2000 rpm for 90 s. Residual salt removal was done by dripping 100 μl of 0.5 M HCl on the coated substrate over the span of 5 s while the wafers were still mounted on the spin coater. The HCl together with the dissolved salt residues were removed by spinning at 2000 rpm for 90 s. The photoresist lift-off was done by acetone while spinning at 2000 rpm, followed by 80 s for drying.

## 2.3 Characterization

X-ray diffraction (XRD) measurements were performed on the precursor MAX phase powder and vacuum-filtered free-standing films, between 3 to 85 $2\theta$ in 0.02° steps using a Malvern Panalytical Aeris diffractometer with CuKa radiation. X-ray photoelectron spectroscopy (XPS) measurements were performed using ESCALAB QXi (Thermo Scientific, USA). High resolution spectra were collected with a pass energy of 20 eV. Valence and cut-off spectra were collected with a pass energy of 5 eV and a bias of −5 V to allow for better energy resolution and clear measurement of the work function. The MXene coatings and patterns were observed by optical microscopy (Motic SMZ 171) and closely examined by high-resolution scanning electron microscopy (HRSEM) at 2 kV (ZEISS Gemini 300). The size distribution of residual salt particles on deposited MXene films were analyzed by image analysis using ImageJ software. Energy-dispersive spectroscopy (EDS) analysis (Bruker X-Flash 6/60) at 15 kV was performed on deposited MXene films using the same HRSEM. A thin lamella containing two regions of interest (ROI) from a 15 μm-wide electrode cross-section was prepared by dual beam focused ion beam (FIB; FEI Helios G4 UC). To protect the ROI surface from the ion beam and enable uniform preparation they were first covered by 500 nm thick electron deposition of platinum followed by 3 μm ion deposition of tungsten covering the whole area. The lamella was examined using a probe Cs-

 

corrected (S-CORR) scanning transmission electron microscope (STEM) (Thermofisher Spectra 200) operating at 200 kV. Atomic force microscopy (AFM) measurements were performed using the MFP-3D-Bio system from Asylum Research/Oxford Instruments. The measurements utilized an AC160TS probe ($f_0 = 300$ kHz, $k = 26$ N m$^{-1}$, nom.) from Olympus, and AC mode was used with a free amplitude ($A_0$) set to 2.34 V (or 200 nm). The setpoint amplitude ($A_s$) was set to 1.423 V (or 125 nm, which is approximately 63% of $A_0$). The operating frequency ($f$) was 283.70 kHz < $f_0$. The in-line transmittance of the glass and MXene-coated glass were measured between the wavelengths of 300–1800 nm by a spectrophotometer through a 5 mm aperture (Agilent Cary 5000).

### 2.4 Electrical measurements

The electrical resistivity and sheet resistance of the pristine n-type Si wafer and uniform MXene coating on sapphire and glass were determined by measuring the voltage induced by applying currents between 10 and 100 μA and 1–10 mA by a four-point probe (Lucas Labs 302, probe distance 1.016 mm) using a 6221 Keithley current source and 2001 multimeter. The measurements were carried out in ambient conditions.

The electrical resistivity of the patterned MXene electrodes was measured using an electric probe system (Keithley 4200A *I–V*/*C–V*) with a four-point probe configuration (probe distance 0.2 mm) using the same Keithley instruments. All measurements were repeated several times at different locations. The MXene–Si Schottky junction diode *I–V* curve characterization was performed using the same Keithley unit with a 2-point probe configuration and 0.04 V steps. The *I–V* curves were measured under various white LED illumination intensities ranging between 270 and 4330 lx determined using a digital LED light meter (HABOTEST HT620L). The illuminance Lux values were converted to irradiance according to 1 lx = 0.0028 W m$^{-2}$ based on measurements on white LEDs.[36] The measurements were carried out in ambient conditions in a cleanroom. All the measurements were repeated while changing the probe placements on various electrodes for validation.

## 3. Results and discussion

### 3.1 MXene deposition and patterning

**3.1.1 Thin-film deposition.** The basic characteristics of the MAX phase precursor and the synthesized MXene are shown in the ESI (Fig. S1).† Control over the spin-coated MXene coverage was achieved by adjusting the MXene solution concentrations and rpm (Fig. S2 and S3†). The MXene coverage improved slightly at a lower spin speed. The distribution was uniform across the wafer besides the considerable accumulation at the rectangular die corners (Fig. S4†). The most influential factor governing coverage is the MXene solution concentration. Above a concentration of 3 g l$^{-1}$, the MXene films start to become continuous. Increasing concentration also results in the presence of more abundant and larger salt residues on the deposited MXene (Fig. S5†). Optimal uniform thin-film formation (>99% coverage) was achieved using a MXene solution concentration of 7 g l$^{-1}$, spun at 2000 rpm. These specific MXene spin-coating parameters were consistently employed for all subsequent experiments conducted in this study.

**3.1.2 Removal of salt residues.** Micropatterned MXene thin films using photolithography-lift-off based techniques were achieved by a simple three-step method (Fig. 1a–c), resulting in clean MXene patterns with few-micron resolution in a streamlined procedure without removing the substrate from the spin coater. After the spin coating deposition many salt residues are observed (Fig. 1d). EDS confirmed that these residue particles contain only F (Fig. S6†) and are therefore assumed to be LiF. Following the HCl spin-cleaning treatment all salt residues, ranging in sizes of ~10–500 nm, were removed (Fig. 1g). Note that the bright white spots are LiF, what remains after the cleaning process are only wrinkles in the MXene. The HCl dissolves the submicron/nano salt particles and is spin dried without any residue accumulation. Since MXene cannot be exfoliated in an acidic solution[37] the film remains intact and unaffected after HCl application. To date, most of the studies that demonstrated fabrication of intricate microelectronic MXene thin-film components employ methods that involve low-concentration solutions such as spray coating and dip coating which are difficult to use at large scales.[18] The HCl spin-cleaning treatment offers high throughput and scalability by enabling MXene deposition with very high concentration colloidal solutions that are produced with less scrutiny and contain more salt impurities. This approach could be implemented for other 2D materials synthesized by intercalation and exfoliation.[3,34,38]

**3.1.3 Patterning by lift-off.** MXene deposits over both the Si and photoresist in an isotropic manner. Using the diluted piranha treatment the Si becomes more hydrophilic in comparison to the photoresist, resulting in full coverage of the Si whereas the photoresist remains partially exposed (Fig. 1e, f and S7, S8a and b†). This allows for simple removal of the photoresist and in turn enables an effective lift-off process. This final step of removing the photoresist is done directly on the spin-coater using acetone, allowing for a seamless and facile process, yielding patterned MXene electrodes (Fig. S7 and S8†). Following the lift-off step, folds 1–2 μm wide can be observed at the edges of the MXene films (Fig. 1h and i). The width of the folds matches the thickness of the photoresist. Performing the lift-off step directly on the spin-coater results in a more controlled and uniform folding as compared to lift-off without spinning (Fig. S9†). The resolution limits in these processes are defined by the photoresist thickness and the average size of the MXene flakes. We demonstrated this process is effective at wafer-scale, at least up to a diameter of 4 inches (Fig. S10†).

### 3.2 Morphological characterization of patterned MXene thin films

The lift-off of the MXene thin-films created some noticeable features in the outline of the patterns (Fig. 2a–c), associated with the nature of the MXene's 2D flake morphology. (1) Standing vertical films of MXene can be observed at the corner edges of patterns (Fig. 1i and 2a). (2) Distinct large wrinkles, oriented in parallel to the MXene pattern edge, persist along

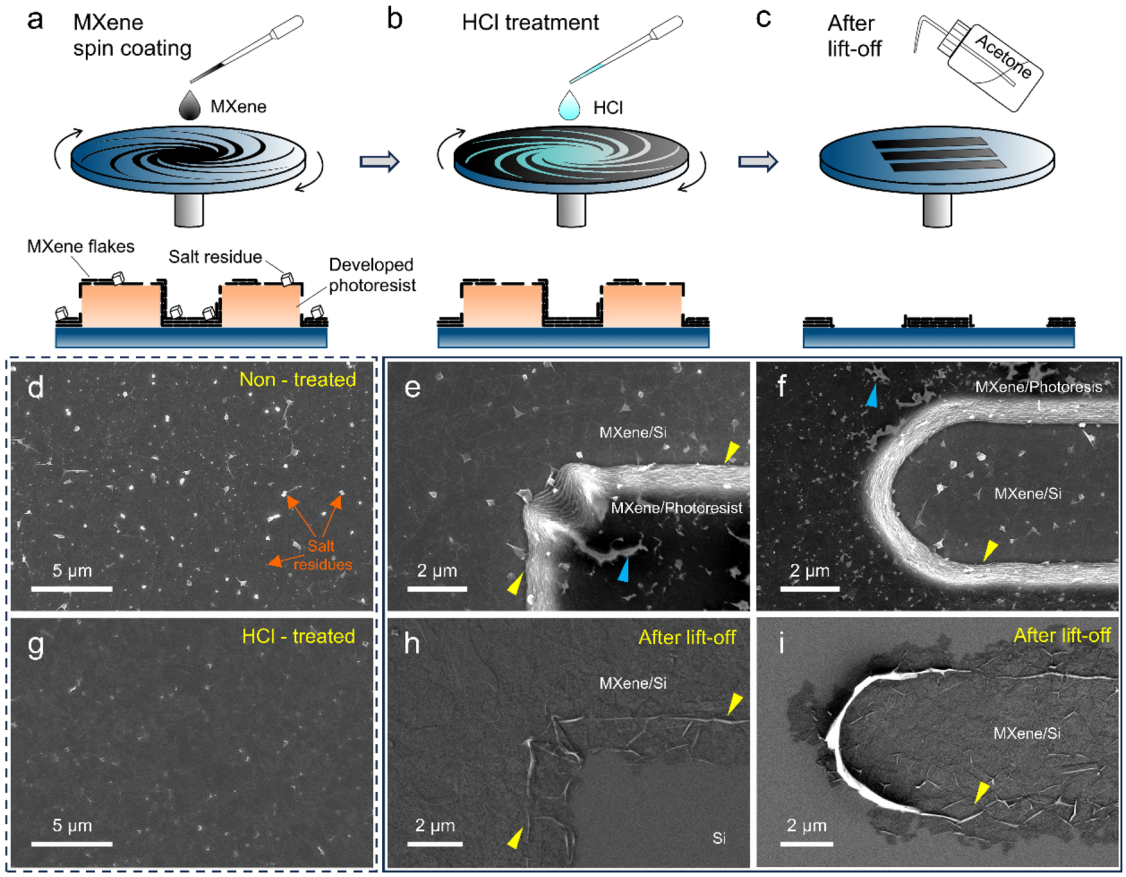


Fig. 1 Three-step process of MXene deposition, salt removal, and thin-film patterning. Schematic illustration of the process steps (a) MXene spin coating over patterned photoresist, (b) salt residue removal by HCl spin-cleaning, and (c) lift-off of the photoresist on the spin coater. SEM images of MXene thin film (d) before and (g) after HCl spin-cleaning. MXene coating on Si and developed photoresist showing a (e) corner and (f) electrode edge, exposed photoresist is indicated by blue arrowheads. MXene patterns after photoresist removal (lift-off) of similar (h) corner and (i) electrode edge. Folding and wrinkling is present at the edges where the photoresist used to be, as indicated by yellow arrowheads.

both sides of the patterned electrode (Fig. 2b, S9g and h†). These wrinkles manifest where the edge of the photoresist used to be (Fig. 1 and S9†). (3) Spill-out or inside-folding of individual flakes is intermittently observed (Fig. 2b and c). The lateral size of these defects is usually 1–1.5 μm. It can be assumed that the formation of the edge imperfections like walls, folds, or spill-outs are sensitive to the photoresist type, thickness, and lift-off process. We suggest that optimizing the photoresist type and height will alleviate or eliminate most of these imperfections. Ultimately, the patterning spatial resolution will be dictated by the size of the MXene flakes. Another consistent feature that is not associated with the lift-off is shallow homogenous ripples in the MXene flakes, which can be observed at high magnifications (Fig. 2c). Despite the common occurrence of ripples in deposited MXenes, the physics behind them is still not fully understood.[39]

The relatively large wrinkles are generally not found in MXene films formed by other means and can reach a height of up to ~60 nm (Fig. 3d), while being only ~10–20 nm wide, owing to the flexibility of MXene flakes.[40] Since the large wrinkles or vertical walls exhibit a large height-to-width aspect ratio, they can perhaps be utilized to study fundamental nanoscale effects for development of optoelectronics, biosensors, energy storage, and more.[41]

The MXene thin film is formed by tiling and intersections of MXene flakes. The intersections between adjacent MXene flakes form line defects that resemble edge dislocations (Fig. 3f). These defects act as "grain boundaries" in the MXene film, which is why increasing flake size enhances electrical conductivity.[40] Therefore, optimizing the flake size in the case of lift-off-based patterning poses a trade-off between improving electrical conductivity or patterning with better lateral resolution, which will be better with larger and smaller flakes, respectively.

AFM measurements were used to analyze the thin-film thickness distribution, indicating an average thickness 3–5 MXene layers (Fig. 3a). The number of layers corresponds with the thickness observed for a single layer ~1.5 nm (Fig. 3c), which agrees with the *d*-spacing of a free-standing film determined by XRD (Fig. 2d). This specific thickness depends on the termination groups, remaining intercalated lithium ions, and water molecules – factors governed by the synthesis method.[42] The average deposited MXene thin-film thickness is about ~6 nm (Fig. 3b). Further AFM measurements confirm the deposition uniformity by sampling a very large area of over ≥1000 $\mu m^2$ in total (Fig. S11†). The AFM scans in high vertical

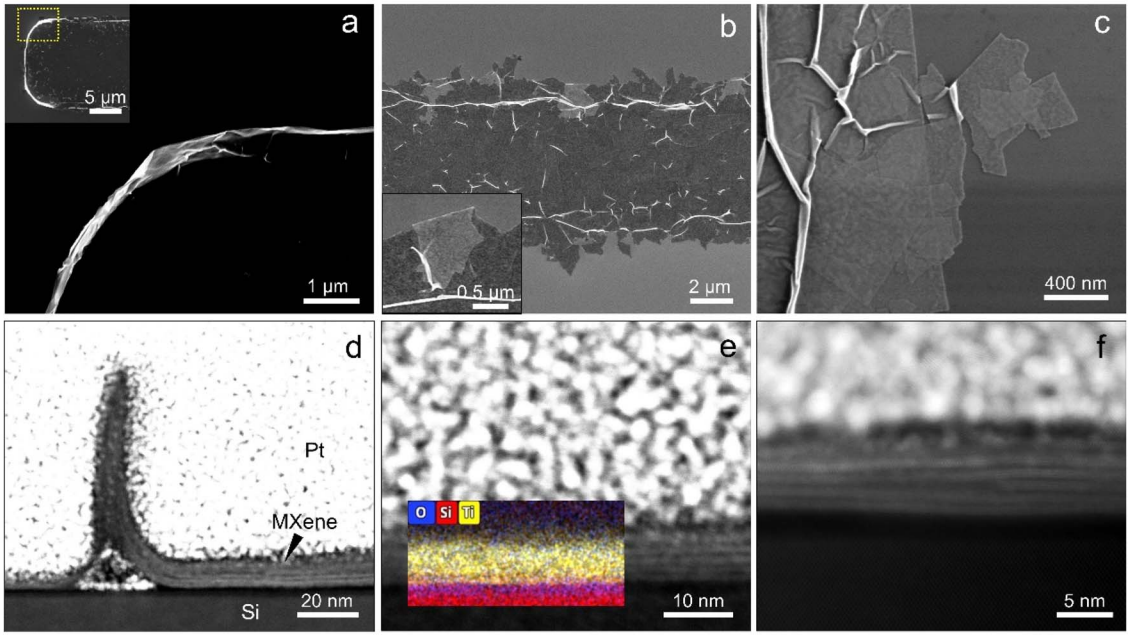


Fig. 2 MXene thin-film pattern imperfections. (a) SEM image of vertical MXene flakes at outlining the corner of a 15 µm electrode, the whole edge area is shown at lower magnification in the insert. (b) SEM image of a 5 µm electrode demonstrating spill-outs and backwards folding of flakes, insert shows a zoom-in on a back-folded flake. (c) High-resolution SEM image showing the relatively large wrinkles, small homogenous ripples in the MXene flakes, and spill-out of a few flakes at a pattern edge. (d) STEM images of the MXene thin-film cross section showcasing (d) a typical large wrinkle fold at the edge of a pattern, (e) typical midsection overlayed with EDS mapping of O (blue), Si (red) and Ti (yellow), and (f) high-resolution image of MXene line defect formed at flake intersections.

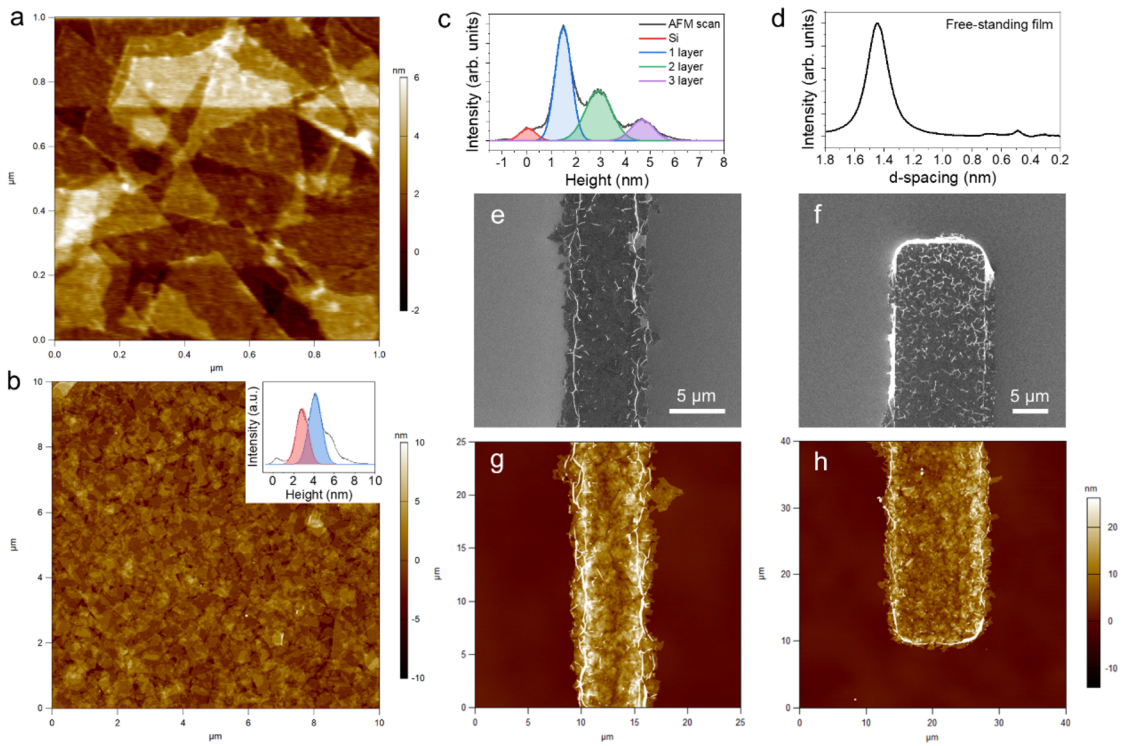


Fig. 3 Analysis of spin-coated MXene thin films thickness. AFM measurements of MXene coating of (a) 1 × 1 and (b) 10 × 10 $\mu m^2$ scan area, (b) inset shows a density plot of the thickness with the red and blue fits corresponding to 2 and 3 MXene flakes, respectively. (c) Density plot of thickness distribution of the scan in (a) with the green, red, and blue fits corresponding to 1, 2, and 3 flakes. (d) XRD spectrum as a function of *d*-spacing for a free-standing MXene film made from the coating solution. SEM images of patterned MXene electrodes with a width of (e) 5 and (f) 15 µm, and corresponding AFM scans of (g) 5 and (h) 15 µm wide electrodes, that share the same color bar scale.

resolution confirm the complete removal of the 3D halide salt residues. For the patterned electrodes the thickness in the uniform areas was found to be either ~6 or ~7.5 nm on average (corresponding to 4 or 5 flakes) (Fig. S11 and S12†). This is also corroborated by TEM analysis of the cross-section (Fig. S13†). Near the edges of the electrodes there is some localized increase in thickness up to ~20–40 nm (Fig. 3g and h) and evens out over the span of about 5 to 10 μm (Fig. S12†). Such increased thickness at electrode edges following lift-off is expected.[18] This increased thickness arises from the aforementioned wrinkles and folds created in MXene flakes upon removal of the photoresist walls. This may pose some limitations to the width of thin-film MXene features with thickness below 10 nm that can be produced using this method.

### 3.3 Optical and electrical properties

Spin-coating of a ~6 nm thin film of MXene was demonstrated on sapphire and glass dies (Fig. 4). The sheet resistance of the MXene coated sapphire was measured at 770 Ω $sq^{-1}$ (Fig. 4c), corresponding to a conductivity of 2164 S $cm^{-1}$. The electrical resistance of MXene films depends on multiple factors: the film thickness, MXene stoichiometry, flakes defects, film packing density, and flake size.[40] The sheet resistance could be increased by enlarging the flake size[21] but doing so will negatively impact the resolution limit of the deposition after photolithography.

To measure the transparency and deposition repeatability of the MXene coatings, glass substrates were coated by single and multiple spin-coating cycles (Fig. 4d). Note that $Ti_3C_2T_z$ MXene absorbs about ~3% of visible light for a single MXene layer.[16,43] After one spin-coating cycle the film absorbs approximately 11.5% at 550 nm, and each additional cycle consistently absorbs another ~10% (Fig. 4d insert), following the expected linear relation of Beer–Lambert law. The absorbance band at around ~800 nm is related to the surface plasmon of $Ti_3C_2T_z$ and the decrease above ~1400 nm is also typical behavior of this material.[29] The measured transparency and sheet resistance of the spin-coated films agree with values measured for $Ti_3C_2T_z$ MXene thin films of similar thickness.[21] Overall, the single-cycle spin-coated films exhibit sufficiently high transparency (~88.5% at 550 nm) and high conductivity (>2000 S $cm^{-1}$) for transparent electronic applications.[17]

The electrical properties of the fabricated electrodes and the MXene–Si junction were probed to assess the performance of the patterned thin films (Fig. 5). The resistance of 50 and 100 μm wide MXene electrodes was 3251 and 1372 Ω, respectively (Fig. 5a). The estimated conductivities based on the approximate electrodes cross-sections (measured by AFM) are ~1350

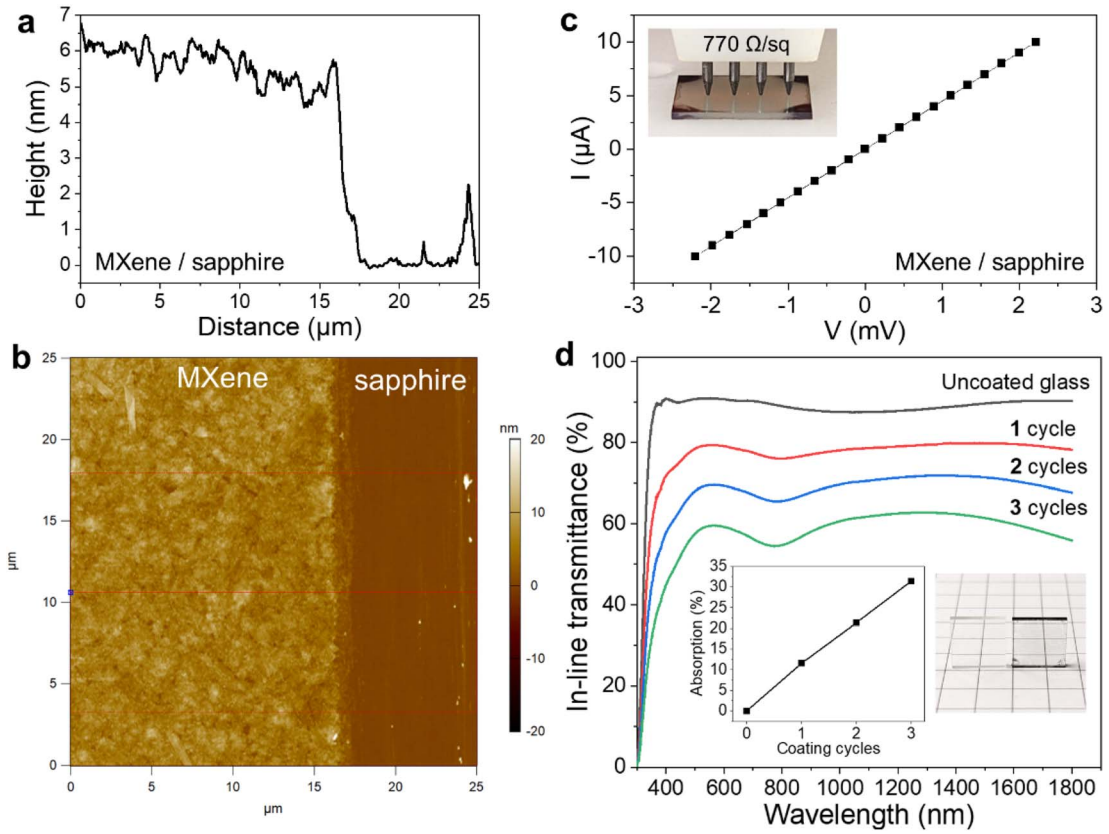


Fig. 4 Transparent uniform spin-coated $Ti_3C_2T_z$ MXene thin films on sapphire and glass. (a) Average height profile of the film corresponding to the area marked in (b) the matching AFM scan. (c) *I*–*V* curve of MXene coated sapphire and an inserted photograph of the sample as measured by the 4-point probe setup. (d) In-line transmittance of MXene-coated glass after up to three spin coating cycles. Inserts show the absorbance values at 550 nm as a function of coating cycles and a photograph of uncoated and spin-coated glass after a single cycle.

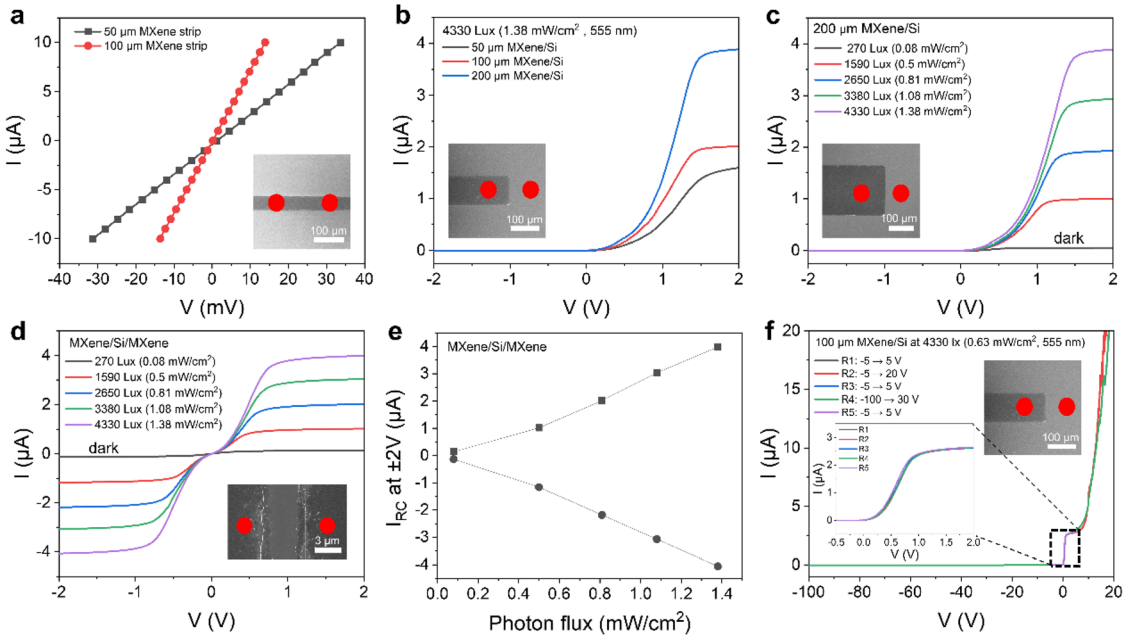


Fig. 5 Electrical properties of patterend MXene electrodes on Si. (a) Four-point probe *I*–*V* measurements of 50 and 100 μm wide electrodes. The insert shows an SEM image of the probed region, and the red dots mark the approximate placement of the probes. (b) *I*–*V* measurements of 50, 100, and 200 μm electrodes serving as Schottky diodes. (c) 200 μm MXene diode under different illumination intensities. (d) Voltage measurements across a MXene–Si–MXene junction under different white light intensities. (e) Recombination current as a function of photon flux for the measurement shown in (d). (f) 100 μm-wide MXene diode *I*–*V* curve before and after operation at relatively high voltages (−100–50 V). Insert shows a zoom-in view of the indicated recombination current region.

and ∼2200 S $cm^{-1}$ for a width of 50 and 100 μm, respectively. These values are in good agreement with the conductivity of MXene thin films measured by others.[44]

$Ti_3C_2T_z$ is a metallic conductor with a work function ranging from 3.9 to 4.8 eV, depending on the termination groups.[14] Using XPS[45] the work function of our MXene was determined to be 4.19 eV (Fig. S1d†). Due to the selection of the n-type Si and the MXene work function, the MXene patterns on Si wafer create van der Waals Schottky diodes. The diode *I*–*V* characteristics depend on the electrode dimensions which determine the MXene–Si contact area (Fig. 5b). The MXene thin film is transparent to visible light and upon increasing the illumination luminous flux from 0.08 to 1.38 mW $cm^{-2}$ increased the recombination current by three orders of magnitude (Fig. 5c). MXene–Si–MXene acts as a 2-terminal planar structure metal–semiconductor–metal (MSM) photodetector. The MSM junction *I*–*V* characteristic of under different illumination intensities exhibits high sensitivity to light under relatively low photon flux (0.08–1.38 mW $cm^{-2}$) (Fig. 5d and e). Although similar observations have been made previously by Kang *et al.*,[46] it was demonstrated under two orders of magnitude higher flux (40–106 mW $cm^{-2}$). The MXene–Si Schottky diode exhibits a low reverse current of 28 nA at −100 V (Fig. 5f). The *I*–*V* characteristics of the diode were not affected after scanning from −100 to 50 V. A zoom-in view illustrates the recombination current barrier region (Fig. 5f). Typically, making photodetectors requires utilizing transparent semiconductors like indium tin oxide (ITO) and ruthenium oxide (RuO) without employing complex fabrication methods involving backside illumination.[32] Alternatively, our method allows fabrication of complex architecture transparent diodes by simple MXene micropatterning at room temperature without any high vacuum deposition. We show that the patterned film thickness and line dimensions can be reduced to several nanometers and ≤100 μm, respectively, without dramatically hindering the MXene performance. The resistance of the MXene remains negligible compared to the MXene–Si–MXene junction, enabling a simple production of transparent MXene electrodes for sensitive photodetectors.[47,48]

## 4. Conclusions

Spin coating is a standard nanofabrication technique that can be employed for deposition of MXene thin films using MXene colloidal solutions. However, the presence of halide salt residues can cause problems during ensuing fabrication processes or device operation. Herein, we present a straightforward approach for controlled deposition and patterning of extremely thin (<10 nm) and halide-residue free 2D MXene features at ambient conditions. The process involves three steps: (1) spin coating for MXene deposition, (2) cleaning halide salt residues by HCl spin-cleaning, and (3) lift-off of a developed photoresist to achieve desired patterns with a lateral resolution of ∼1.5 μm. The deposition process is repeatable and can be done consecutively to achieve targeted film thickness. The patterned MXene was thoroughly characterized by high resolution electron microscopy and AFM. The transparent electrodes exhibited conductivities of approximately 1300 and 2200 S $m^{-1}$, for a width of 100 and 50 μm, respectively. The MXene–Si Schottky

diode characteristics were assessed and displayed high sensitivity to light under a photon flux of 0.08–1.38 mW $cm^{-2}$. The combination of spin-coating followed by HCl spin-cleaning to eliminate salt residues offers significant advantages, addressing one of the main drawbacks associated with deposition of MXene films.

## Data availability

The data supporting the findings of this study are available from the corresponding author upon reasonable request. Specific datasets, including experimental protocols, characterization data, and analysis results, can be provided to researchers with legitimate interests in replicating or expanding upon this work.

## Conflicts of interest

The authors declare there are no conflicts to declare.

## Acknowledgements

This work was supported by the Israel Science Foundation (grant No. 2527/22).

## References

1 P. R. Morris, A History of the World Semiconductor Industry, *A History of the World Semiconductor Industry*, 1990, DOI: 10.1049/PBHT012E.
2 H. Wang, Z. Yao, L. Acauan, J. Kong and B. L. Wardle, Toward MXene interconnects, *Matter*, 2021, **4**, 1447–1449.
3 Z. Lin, Y. Huang and X. Duan, Van der Waals thin-film electronics, *Nat. Electron.*, 2019, **2**(9), 378–388.
4 J. H. Kim, *et al.*, Centimeter-scale Green Integration of Layer-by-Layer 2D TMD vdW Heterostructures on Arbitrary Substrates by Water-Assisted Layer Transfer, *Sci. Rep.*, 2019, **9**(1), 1–10.
5 R. Kumar, B. Kumari, S. Kumar, M. Sahoo and R. Sharma, Temperature and Dielectric Surface Roughness dependent Performance Analysis of Cu-Graphene Hybrid Interconnects, *IEEE Electrical Design of Advanced Packaging and Systems Symposium 2020-December*, 2020.
6 X. Chen, *et al.*, Fully integrated graphene and carbon nanotube interconnects for gigahertz high-speed CMOS electronics, *IEEE Trans. Electron Devices*, 2010, **57**, 3137–3143.
7 X. Liang, *et al.*, Toward clean and crackless transfer of graphene, *ACS Nano*, 2011, **5**, 9144–9153.
8 Y. Gogotsi and B. Anasori, The Rise of MXenes, *ACS Nano*, 2019, **13**, 8491–8494.
9 B. Anasori and Y. Gogotsi, 2D Metal carbides and nitrides (MXenes): Structure, properties and applications, *2D Metal Carbides and Nitrides (MXenes): Structure, Properties and Applications*, 2019, pp. 1–534, DOI: 10.1007/978-3-030-19026-2/COVER.
10 A. Moscatelli, The pull of the MXene vortex, *Nat. Nanotechnol.*, 2022, **17**, 1025.
11 K. R. G. Lim, *et al.*, Fundamentals of MXene synthesis, *Nat. Synth.*, 2022, **1**(8), 601–614.
12 C. E. Shuck, *et al.*, Scalable Synthesis of Ti3C2Tx MXene, *Adv. Eng. Mater.*, 2020, **22**, 1901241.
13 J. H. Moon, *et al.*, Materials Quest for Advanced Interconnect Metallization in Integrated Circuits, *Advanced Science*, 2023, **10**, 2207321.
14 T. Schultz, *et al.*, Surface Termination Dependent Work Function and Electronic Properties of Ti3C2Tx MXene, *Chem. Mater.*, 2019, **31**, 6590–6597.
15 J. L. Hart, *et al.*, Control of MXenes' electronic properties through termination and intercalation, *Nat. Commun.*, 2019, **10**(1), 1–10.
16 T. Yun, *et al.*, Electromagnetic Shielding of Monolayer MXene Assemblies, *Adv. Mater.*, 2020, **32**, 1906769.
17 K. Hantanasirisakul, *et al.*, Fabrication of Ti3C2Tx MXene Transparent Thin Films with Tunable Optoelectronic Properties, *Adv. Electron. Mater.*, 2016, **2**, 1600050.
18 X. Xu, T. Guo, M. Lanza and H. N. Alshareef, Status and prospects of MXene-based nanoelectronic devices, *Matter*, 2023, **6**, 800–837.
19 Z. Wang, H. Kim and H. N. Alshareef, Oxide Thin-Film Electronics using All-MXene Electrical Contacts, *Adv. Mater.*, 2018, **30**, 1706656.
20 M. Mojtabavi, *et al.*, Wafer-Scale Lateral Self-Assembly of Mosaic Ti3C2TxMXene Monolayer Films, *ACS Nano*, 2021, **15**, 625–636.
21 T. Guo, *et al.*, Rational Design of Ti3C2Tx MXene Inks for Conductive, Transparent Films, *ACS Nano*, 2023, **17**, 3737–3749.
22 C. J. Zhang, *et al.*, Additive-free MXene inks and direct printing of micro-supercapacitors, *Nat. Commun.*, 2019, **10**(1), 1–9.
23 M. Mariano, *et al.*, Solution-processed titanium carbide MXene films examined as highly transparent conductors, *Nanoscale*, 2016, **8**, 16371–16378.
24 X. Xu, *et al.*, High-Yield Ti3C2Tx MXene–MoS2 Integrated Circuits, *Adv. Mater.*, 2022, **34**, 2107370.
25 K. Montazeri, *et al.*, Beyond Gold: Spin-Coated Ti3C2-Based MXene Photodetectors, *Adv. Mater.*, 2019, **31**, 1903271.
26 Q. Jiang, *et al.*, On-Chip MXene Microsupercapacitors for AC-Line Filtering Applications, *Adv. Energy Mater.*, 2019, **9**, 1901061.
27 E. Kim, *et al.*, Scalable fabrication of MXene-based flexible micro-supercapacitor with outstanding volumetric capacitance, *Chem. Eng. J.*, 2022, **450**, 138456.
28 B. Xu, *et al.*, Ultrathin MXene-Micropattern-Based Field-Effect Transistor for Probing Neural Activity, *Adv. Mater.*, 2016, **28**, 3333–3339.
29 A. Hazan, *et al.*, MXene-Nanoflakes-Enabled All-Optical Nonlinear Activation Function for On-Chip Photonic Deep Neural Networks, *Adv. Mater.*, 2023, **35**, 2210216.
30 S. Ahn, *et al.*, A 2D Titanium Carbide MXene Flexible Electrode for High-Efficiency Light-Emitting Diodes, *Adv. Mater.*, 2020, **32**, 2000919.

31 K. A. Reinhardt and W. Kern, *Handbook of Silicon Wafer Cleaning Technology*, 3rd edn, 2018, pp. 1–773, DOI: 10.1016/C2016-0-01001-X.
32 L. Luo, *et al.*, MXene-GaN van der Waals metal-semiconductor junctions for high performance multiple quantum well photodetectors, *Light: Sci. Appl.*, 2021, **10**(1), 1–11.
33 G. Li, *et al.*, Terahertz Polarizers Based on 2D Ti3C2Tz MXene: Spin Cast from Aqueous Suspensions, *Adv. Photonics Res.*, 2020, **1**, 2000084.
34 B. Li, *et al.*, Patterning of Wafer-Scale MXene Films for High-Performance Image Sensor Arrays, *Adv. Mater.*, 2022, **34**, 2201298.
35 D. Lee, *et al.*, Centrifugal-Gravity-Enforced Deposition of MXene Electrodes for High-Performance and Ultrastable Microsupercapacitors, *ACS Appl. Mater. Interfaces*, 2024, **16**, 26004–26014.
36 P. R. Michael, D. E. Johnston and W. A. Moreno, Calculation of Irradiance from Illuminance for Artificial Light Photovoltaics Applications, *IEEE Instrum. Meas. Mag.*, 2023, **26**, 52–58.
37 V. Natu, M. Sokol, L. Verger and M. W. Barsoum, Effect of Edge Charges on Stability and Aggregation of Ti3C2T z MXene Colloidal Suspensions, *J. Phys. Chem. C*, 2018, **122**, 27745–27753.
38 O. Song, *et al.*, All inkjet-printed electronics based on electrochemically exfoliated two-dimensional metal, semiconductor, and dielectric, *npj 2D Mater. Appl.*, 2022, **6**(1), 1–12.
39 A. Sarycheva, M. Shanmugasundaram, A. Krayev and Y. Gogotsi, Tip-Enhanced Raman Scattering Imaging of Single- to Few-Layer Ti3C2TxMXene, *ACS Nano*, 2022, **16**, 6858–6865.
40 J. Zhang, *et al.*, Scalable Manufacturing of Free-Standing, Strong Ti3C2Tx MXene Films with Outstanding Conductivity, *Adv. Mater.*, 2020, **32**, 2001093.
41 T. E. Song, *et al.*, Vertically Aligned Nanopatterns of Amine-Functionalized Ti3C2 MXene *via* Soft Lithography, *Adv. Mater. Interfaces*, 2020, **7**, 2000424.
42 V. Natu, *et al.*, Effect of Base/Nucleophile Treatment on Interlayer Ion Intercalation, Surface Terminations, and Osmotic Swelling of Ti3C2TzMXene Multilayers, *Chem. Mater.*, 2022, **34**, 678–693.
43 A. D. Dillon, *et al.*, Highly Conductive Optical Quality Solution-Processed Films of 2D Titanium Carbide, *Adv. Funct. Mater.*, 2016, **26**, 4162–4168.
44 A. Lipatov, *et al.*, Effect of Synthesis on Quality, Electronic Properties and Environmental Stability of Individual Monolayer Ti3C2 MXene Flakes, *Adv. Electron. Mater.*, 2016, **2**, 1600255.
45 J. E. Whitten, Ultraviolet photoelectron spectroscopy: Practical aspects and best practices, *Appl. Surf. Sci. Adv.*, 2023, **13**, 100384.
46 Z. Kang, *et al.*, MXene–Silicon Van Der Waals Heterostructures for High-Speed Self-Driven Photodetectors, *Adv. Electron. Mater.*, 2017, **3**, 1700165.
47 F. H. L. Koppens, *et al.*, Photodetectors based on graphene, other two-dimensional materials and hybrid systems, *Nat. Nanotechnol.*, 2014, **9**(10), 780–793.
48 L. Li and G. Shen, MXene based flexible photodetectors: progress, challenges, and opportunities, *Mater. Horiz.*, 2023, **10**, 5457–5473.